Control of rectification and permeation by two distinct sites after the second transmembrane region in Kir2.1 K^+ channel

Yoshihiro Kubo*†‡ and Yoshimichi Murata†

*Department of Neurophysiology, Tokyo Metropolitan Institute for Neuroscience, Tokyo 183-8526, †Department of Physiology, Tokyo Medical and Dental University, Graduate School and Faculty of Medicine, Tokyo 113-8519 and ‡CREST, Japan Science and Technology Corporation, Saitama 332-0012, Japan

(Received 28 September 2000; accepted after revision 1 November 2000)

1. The rectification property of the inward rectifier K^+ channel is chiefly due to the block of outward current by cytoplasmic Mg^{2+} and polyamines. In the cloned inward rectifier K^+ channel Kir2.1 (IRK1), Asp172 in the second transmembrane region (M2) and Glu224 in the putative cytoplasmic region after M2 are reported to be critical for the sensitivity to these blockers. However, the difference in the inward rectification properties between Kir2.1 and a very weak inward rectifier sWIRK could not be explained by differences at these two sites.

2. Following sequence comparison of Kir2.1 and sWIRK, we focused this study on Glu299 located in the centre of the putative cytoplasmic region after M2. Single-point mutants of Kir2.1 (Glu224Gly and Glu299Ser) and a double-point mutant (Glu224Gly–Glu299Ser) were made and expressed in *Xenopus* oocytes or in HEK293T cells.

3. Their electrophysiological properties were compared with those of wild-type (WT) Kir2.1 and the following observations were made. (a) Glu299Ser showed a weaker inward rectification, a slower activation upon hyperpolarization, a slower decay of the outward current upon depolarization, a lower sensitivity to block by cytoplasmic spermine and a smaller single-channel conductance than WT. (b) The features of Glu224Gly were similar to those of Glu299Ser. (c) In the double mutant (Glu224Gly–Glu299Ser), the differences from WT described above were more prominent.

4. These results demonstrate that Glu299 as well as Glu224 control rectification and permeation, and suggest the possibility that the two sites contribute to the inner vestibule of the channel pore. The slowing down of the on- and off-blocking processes by mutation of these sites implies that Glu224 and Glu299 function to facilitate the entry (and exit) of spermine to (and from) the blocking site.

The inward rectification property of the inward rectifier K^+ channel has been reported to be due to block of the outward current by intracellular magnesium (Mg_i^{2+}) (Matsuda *et al.* 1987; Vandenberg, 1987; Matsuda, 1988) and by cytoplasmic polyamines (Lopatin *et al.* 1994; Ficker *et al.* 1994; Fakler *et al.* 1995; Ishihara *et al.* 1996). The structural elements that determine the inward rectification property were identified using mutagenesis studies (reviewed in Nichols & Lopatin, 1997). The first site to be tested was Asp (D) at position 172 of Kir2.1 (IRK1) in the M2 region (Fig. 1*A*). By mutating this site to Asn (N), the sensitivity to block by polyamines and Mg_i^{2+} was significantly reduced (Lu & MacKinnon, 1994; Stanfield *et al.* 1994; Wible *et al.* 1994), and the activation phase that reflects the unblocking of the spermine blockage disappeared. Thus, this site was thought to have a strong energetic contribution to the binding (and pore plugging) of the blockers. In 1995, Glu (E) at position 224 of Kir2.1 in the putative cytoplasmic chain after M2 was identified as having an influence on the inward rectification property (Yang *et al.* 1995; Taglialatela *et al.* 1995). Yang *et al.* (1995) also showed that the mutation of E at position 224 to Gly (G) (E224G) affected the permeation properties such as the single-channel conductance and the open channel noise.

We previously isolated a weak inward rectifier K^+ channel from the salmon brain (sWIRK) (Kubo *et al.* 1996), whose primary structure showed similarities with mammalian Kir4.1 (BIR10/K_{AB}-2) (Bond *et al.* 1994; Takumi *et al.* 1995). In spite of the existence of a negatively charged amino acid (E179) in the middle of the

M2 region, which corresponds to D172 of Kir2.1, sWIRK showed a very weak rectification (Kubo *et al.* 1996). The amino acid residue that corresponds to E224 of Kir2.1 is G231, as for Kir1.1 (G223). By mutating E179 of sWIRK to Gln (Q) (E179Q, G231), the inward rectification property was almost completely lost and it showed outward rectification even in the presence of cytoplasmic blockers (Kubo *et al.* 1996). As this feature clearly differed from the double mutant of Kir2.1 (D172N–E224G) (Yang *et al.* 1995) or from WT Kir1.1 (N171, G223; Ho *et al.* 1993), the presence of an additional site(s) in Kir2.1 and Kir1.1 critical for the strong inward rectification was speculated. Therefore, the amino acid sequence of sWIRK was compared in this study with that of other strong inward rectifiers such as Kir2.1, and E299 of Kir2.1 almost half-way through the putative cytoplasmic region following the M2 region was focused upon (Fig. 1*A* and *B*). The corresponding amino acid residues were negatively charged in all strong inward rectifiers and in Kir1.1, which also showed strong rectification when a negatively charged amino acid was introduced into the M2 region (N171D) (Lu & MacKinnon, 1994). In contrast, the corresponding residue was Ser in sWIRK, in Kir4.1 and in Kir7.1 (Fig. 1*B*). Single-, double- and triple-point mutants of Kir2.1 at the three sites D172, E224 and E299 were made, and their electrophysiological properties were compared with those of WT Kir2.1. Preliminary results from this study have been published in abstract form (Kubo, 1999).

METHODS

In vitro mutagenesis

The single-point mutants were made using the Sculptor kit (Amersham), using mutated oligonucleotide DNA primers and single-stranded (ss)DNA of WT mouse Kir2.1. The introduction of a mutation was confirmed by sequencing with a PRISM kit (Applied Biosystems) using ABI 377-18 DNA sequencer (Applied Biosystems). The electrophysiological properties of two independent clones of the mutant were confirmed to be identical. The double-point mutants were made using the ssDNA of the single-point mutants, and the triple mutants were prepared based on the ssDNA of the double mutants.

Two-electrode voltage-clamp recordings in *Xenopus* oocytes

Xenopus oocytes were collected from frogs anaesthetized in water containing 0.15% tricaine; after the final collection the frogs were killed by decapitation. Isolated oocytes were treated with collagenase (2 mg ml^{-1}, type 1, Sigma), and injected with approximately 50 nl of cRNA solution, prepared from the linearized plasmid DNA by RNA transcription kit (Stratagene). The injected oocytes were incubated for 2–4 days in frog Ringer solution (Kubo *et al.* 1993*a*) supplemented with 20 mM KCl at 17 °C. Macroscopic current was recorded under two-electrode voltage clamp using a 'bath-clamp' amplifier (OC-725B-HV, Warner Co.). Stimulation, data acquisition and analysis were done on a Pentium-based computer using Digidata 1200A and pCLAMP software (Axon Instruments). Intracellular glass microelectrodes were filled with 3 M potassium acetate with 10 mM KCl (pH 7.2). The microelectrode resistance ranged from 0.1 to 0.4 MΩ. Two Ag–AgCl pellets (Warner Co.) were used to pass the bath current and to sense the bath voltage. The voltage-sensing electrode was placed near the oocyte (approximately 2 mm away) on the same side as the voltage-recording microelectrode. The bath current-passing pellet and the current injection microelectrode were placed on the other side. Under these conditions, the series resistance between the oocyte surface and the bath voltage-sensing pellet was approximately 200 Ω (Sabirov *et al.* 1997). As the measured current at the most hyperpolarized potential was 50 μA in the largest case, and mostly less than 20 μA, the voltage-clamp error due to this series resistance was estimated to be no more than 10 mV and mostly less than 4 mV. The error, which was not compensated in the experiments, did not change the conclusions of the comparison of WT and mutant channels in the present study. The recording bath solution contained 10 mM KCl, 80 mM *N*-methyl-glucamine, 70 mM

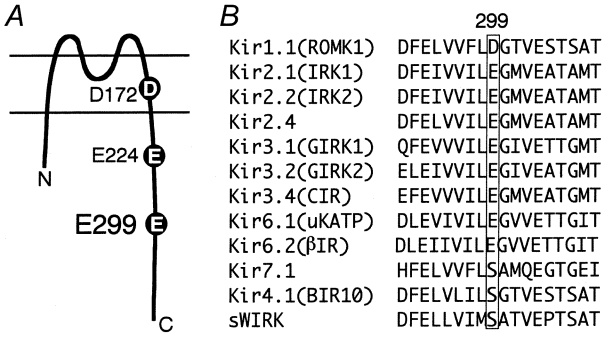

Figure 1. The position of E299 of Kir2.1, and comparison of the corresponding amino acid residues among the inwardly rectifying K^+ channel family

A, schematic drawing of the structure of the Kir2.1 channel based on the initial model by Kubo *et al.* (1993*a*). E299 is located at the centre of the putative cytoplasmic chain after the M2 region. D172 in the M2 region and E224 just after M2 are also depicted. *B*, alignment of the amino acid sequences of the inwardly rectifying K^+ channel family at E299 of Kir2.1 and the surrounding region. The original reports used for the alignment are as follows. Kir1.1, Ho *et al.* (1993); Kir2.1, Kubo *et al.* (1993*a*); Kir2.2, Koyama *et al.* (1994); Kir2.4, Topert *et al.* (1998); Kir3.1, Kubo *et al.* (1993*b*) and Dascal *et al.* (1993); Kir3.2, Lesage *et al.* (1994); Kir3.4, Krapivinsky *et al.* (1995) and Iizuka *et al.* (1995); Kir6.1, Inagaki *et al.* (1995*b*); Kir6.2, Inagaki *et al.* (1995*a*); Kir7.1, Krapivinsky *et al.* (1998) and Doring *et al.* (1998); Kir4.1, Bond *et al.* (1994) and Takumi *et al.* (1995); sWIRK, Kubo *et al.* (1996).

HCl, 3 mM $MgCl_2$ and 5 mM Hepes (pH 7.4). All recordings were carried out at room temperature (23 ± 2 °C).

By assuming the intracellular potassium concentration ($[K^+]_i$) of the oocytes to be 80 mM, the equilibrium potential of the potassium ion (E_K) was calculated to be −52 mV. However, the exact values of $[K^+]_i$ and E_K of each oocyte are unknown. Therefore, E_K, used for the calculation of the chord conductance (Figs 2, 3 and 10) was adjusted to yield a continuous conductance–voltage (g–V) plot. The adjusted E_K ranged from −54 to −49 mV.

Data from the same batch of oocytes were used for comparison of the phenotypes in Figs 2–6 and 10, because properties such as inward rectification and blocking speed are influenced by the cytoplasmic polyamine concentration, and because they differ significantly depending on the batch. Similar tendencies of the data in Figs 2–6 and 10 were reproducibly observed in five batches of oocytes.

Single-channel recordings in *Xenopus* oocytes

For single-channel recording, the vitelline membrane was peeled off by bathing oocytes in a high osmolarity solution (Kubo *et al.* 1993*a*) for 5–10 min. The patch pipettes were prepared from borosilicate glass (Warner Instruments) using a P-97 horizontal puller (Sutter) and a fire polisher (Narishige, Japan). Recordings were obtained under the cell-attached configuration using an Axopatch-1D amplifier (Axon Instruments). The current was low-pass filtered at 1 kHz by a Bessel filter built into the amplifier, and was digitized at 5 kHz. The recordings shown in Fig. 9*A* were digitally filtered at 200 Hz. The pipette (extracellular) and the bath solution contained 136 mM KCl, 3 mM $MgCl_2$, 10 mM Hepes and 4 mM KOH (pH 7.4). The patch pipette resistance ranged from 3 to 10 MΩ.

Expression in HEK293T cells

The cDNAs of WT and mutant Kir2.1 were subcloned into the expression vector $pCXN_2$ (Niwa *et al.* 1991). The plasmid DNA was transfected into HEK293T cells (human embryonic kidney cell line) using Lipofectamine Plus (Gibco BRL) following the manufacturer's protocol. Enhanced green fluorescent protein (GFP; Clontech; 1/10 the amount of plasmid DNA) was co-transfected as a transfection marker. The cells were cultured in Dulbecco's modified Eagle's medium with 10% bovine calf serum for 24 h. The cells were then dissociated by treatment with 0.2% trypsin in Ca^{2+}-, Mg^{2+}-free PBS, and re-seeded on coverslips at a relatively low density. The re-seeding was done to obtain well-isolated cells and to facilitate successful giga-ohm seal formation. It was confirmed that the trypsin treatment did not change the electrophysiological properties of the expressed channels. Electrophysiological recordings were carried out 4–30 h after re-seeding, which corresponds to 28–54 h after transfection.

Macroscopic current recordings in HEK293T cells

A coverslip of HEK293T cells was placed in a recording chamber containing bath solution (see below) on an inverted fluorescence microscope (IX70, Olympus, Japan), and transfected cells were identified by the fluorescence signal of the co-transfected GFP. The macroscopic current was recorded under the excised inside-out patch condition using an Axopatch-1D amplifier. The resistance of the patch pipettes ranged from 2 to 4 MΩ. Fifty to eighty per cent of the voltage error due to the series resistance was compensated by a circuit in the amplifier. The combination of HEK293T cells and the $pCXN_2$ expression vector enabled high expression sufficient for macroscopic current recording using standard-sized patch pipettes. The current was low-pass filtered at 1 kHz by a built-in circuit in the amplifier and digitized at 5 kHz.

The pipette (extracellular side) solution contained 16 mM KCl, 120 mM *N*-methyl-glucamine, 103 mM HCl, 3 mM $MgCl_2$, 10 mM Hepes and 4 mM KOH (pH 7.4). The bath (intracellular side) solution with various concentrations of Mg^{2+} or spermine was prepared as described by Ishihara *et al.* (1996) with some modifications. Mg^{2+}- and spermine-free solution contained 110 mM KCl, 10 mM KH_2PO_4, 2 mM EDTA, 5 mM Hepes, 1.9 mM K_2ATP and 16.35 mM KOH (pH 7.2). K_2ATP was added before use and the solution was used only for the day. The free Mg^{2+} concentration was changed by adding $MgCl_2$, and it was calculated by the method by Fabiato & Fabiato (1979). The amount of added $MgCl_2$ (and the free Mg^{2+} concentration) was as follows: 1.0 mM (2.9 μM), 2.4 mM (33 μM), 3.8 mM (313 μM) and 6.8 mM (2.96 mM). The negative shift of pH by added $MgCl_2$ was adjusted to pH 7.2 by applying KOH of less than 2 mM. Spermine (Sigma) was simply added to the solution just before the experiments and solutions containing spermine were used for up to 2 h. The concentration of added spermine is indicated in Fig. 8. Due to the binding of spermine to ATP (Watanabe *et al.* 1991), the effective concentrations were estimated to be lower than the indicated values. The total $[K^+]_o$ and $[K^+]_i$ were approximately 20 and 140 mM, respectively. The liquid junction potential between the pipette solution and the bath solution was measured to be approximately 10 mV, and membrane potentials were corrected for this value.

The extent of run-down during a set of I–V relationship recordings was monitored by applying step pulses again, and data with apparent run-down were discarded. Due to this limitation, it was not possible to obtain a series of data for all concentrations of blockers from one patch, and the data shown in Figs 7 and 8 were obtained from multiple patches.

RESULTS

Macroscopic current recordings of WT and mutant Kir2.1

The electrophysiological properties of a point mutant of Kir2.1 in which Glu at position 299 was mutated to Ser (E299S) were compared with those of WT Kir2.1 and the D172N and E224G mutants (Fig. 2). The properties of the double mutants of the three sites, D172N–E224G, D172N–E299S and E224G–E299S, were also analysed (Fig. 3). The macroscopic currents in 10 mM K^+ under two-electrode voltage clamp in *Xenopus* oocytes are shown in Figs 2*A* and 3*A*. The current–voltage (I–V) relationships (Figs 2*B* and 3*B*) and the conductance–voltage (g–V) relationships (Figs 2*C* and 3*C*) are also shown.

The observed features were as follows. (1) The D172N mutation weakened the inward rectification slightly, and removed the activation phase upon hyperpolarization (Figs 2 and 3). (2) Both the E224G and E299S mutations remarkably weakened the inward rectification of WT Kir2.1 and the D172N mutant. In the E224G and E299S mutants, significant outward currents were observed even 100 ms after the beginning of the depolarized pulses. Both of the mutations slowed down the activation upon hyperpolarization and the decay of the outward current upon depolarization (Figs 2 and 3). (3) The properties of the E224G and E299S mutants were highly similar to each other (Figs 2 and 3). (4) The double mutation E224G–E299S enhanced the changes observed in the E224G and E299S mutants (Fig. 3).

In the following sections, the properties of WT and mutant channels were compared with respect to inward

rectification, activation at hyperpolarized potentials and decay of the outward current at depolarized potentials.

Comparison of the inward rectification properties of WT and mutant Kir2.1

The intensity of the inward rectification of WT Kir2.1 and the D172N, E224G, E299S and E224G–E299S mutants is compared in Fig. 4. As the conductance of the E224G–E299S double mutant did not reach a plateau level even at the most hyperpolarized potential (Fig. 3*C*), it was not possible to fit the g–V plot reliably with the Boltzmann equation and to compare the fitting parameters quantitatively. Instead, the intensity of the inward rectification was compared semi-quantitatively by normalizing the current amplitudes to the values at −100 mV (Fig. 4*A* and *B*). As an index of the intensity of the inward rectification, the ratio of the current amplitudes at +50 and −100 mV was calculated, and the accumulated data ($n = 3$–4) are shown (Fig. 4*C* and *D*). It is clear that the D172N mutant showed slightly weaker inward rectification than WT, and both E224G and E299S mutants showed much less intense inward rectification. The inward rectification of E224G–E299S, especially at 5 ms from the beginning of the step pulses, was even weaker than that of the E224G or E299S mutants (Fig. 4).

It was additionally observed that E224G–E299S and E224G–E299Q had similar inward rectification properties, and that D172N–E299S and D172N–E299Q were also similar (Fig. 4*C* and *D*). These results imply that the negative charge of E299 contributes to inward rectification and that the changed phenotype of E299S is not due to Ser itself, and similarly in the case of the E224G mutant (Yang *et al.* 1995). However, as there was a difference in the inward rectification properties between E299S and E299Q (Fig. 4*C* and *D*), supplementary effects of the size and the shape of the amino acid residue at position 299

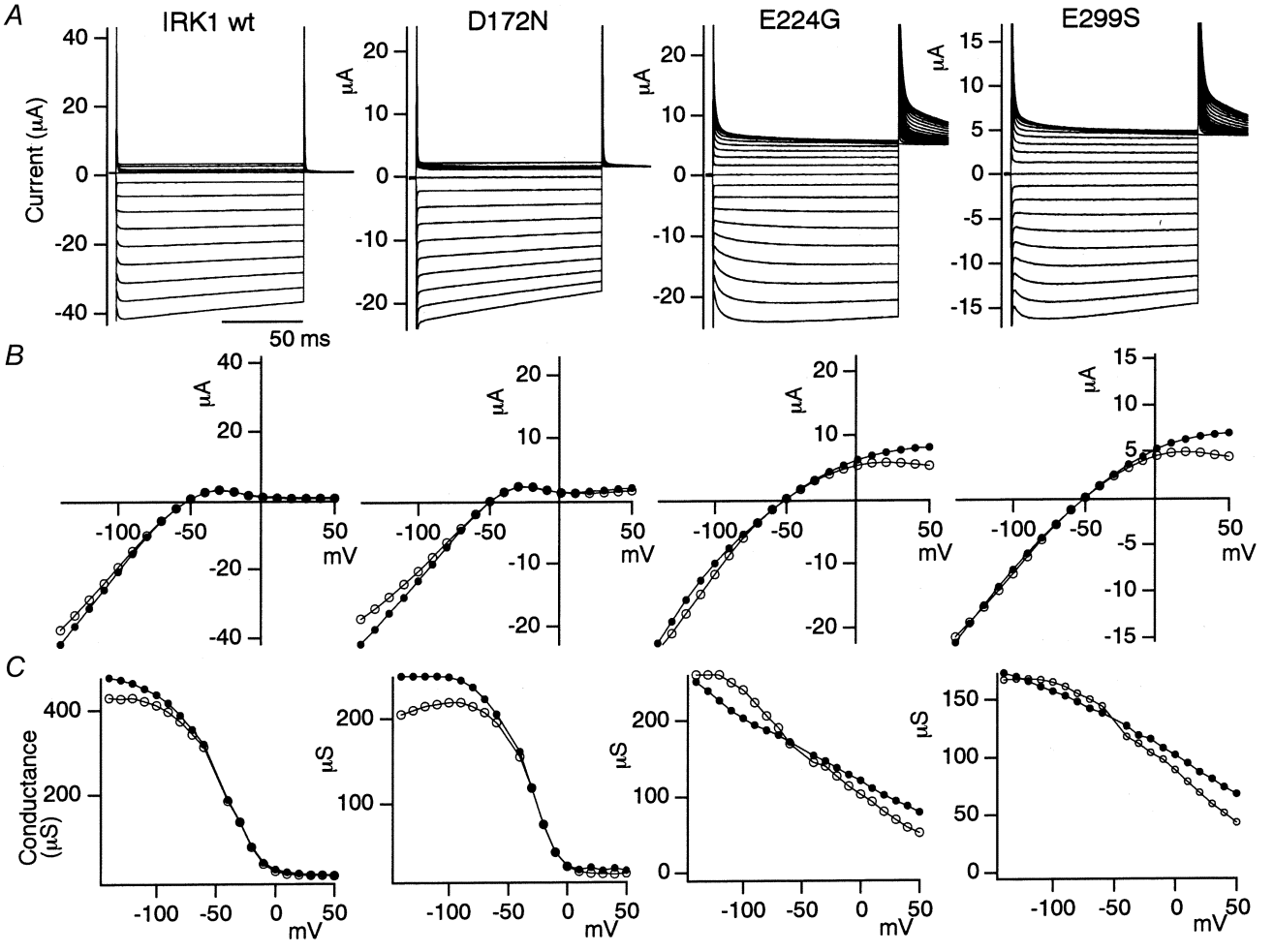

Figure 2. Macroscopic current recordings under two-electrode voltage clamp of WT Kir2.1 (IRK1) and D172N, E224G and E299S mutants expressed in *Xenopus* oocytes

A, representative current recordings in 10 mM K^+_o. The holding potential was −50 mV, and step pulses from +50 to −140 mV were applied by 10 mV decrements. *B*, *I*–*V* relationships of the data in *A*. The current amplitudes at 5 ms (●) and at 100 ms (○) of the step pulses are plotted. *C*, chord g–V relationship of the data in *B*.

were suggested, in addition to the negative charge. To examine further the effect of electrostatic charge at this residue, E299R and E299K mutants were also prepared. Neither of them, however, expressed functional current, showing the importance of the amino acid residue at position 299 for channel function. For the following analysis, E299S was used as a representative mutation of this site.

Comparison of the activation kinetics of WT and mutant Kir2.1

The activation phase upon hyperpolarization was not clearly observed in the D172N (Fig. 2*A*), D172N–E224G or D172N–E299S mutants (Fig. 3*A*). The activation phases at −120 to −160 mV in 10 mM K_o^+ of WT Kir2.1 and the E224G, E299S and E224G–E299S mutants are shown in Fig. 5*A*. The time constants of the fits with a single-exponential function are plotted in Fig. 5*B*. The inactivating component of WT Kir2.1 (Fig. 5*A*) was ignored in the fitting. Fitting with a double-exponential function was also done for E224G–E299S to improve the fit, and the two time constants were also plotted (Fig. 5*B*). The activation of E224G and E299S is clearly slower than that of WT. In E224G–E299S, an additional very slow component was observed. The voltage dependency of the time constants did not differ remarkably between WT and the mutants. These features were confirmed in three oocytes of the same batch, and a similar tendency was reproducibly observed in other batches.

Comparison of the outward current of WT and mutant Kir2.1

The time course of the tail currents at +50 mV, when depolarized from various prepulse potentials, was analysed. In Fig. 6*A*, recordings of the outward current are shown on a magnification scale normalized to the amplitude of the inward current at −100 mV. The decay of the outward current of WT Kir2.1 was too fast to be analysed separately from the capacitative current. In contrast, the tail currents of the mutants were larger in amplitude and declined much more slowly. They could be fitted not with a single- but with a double-exponential

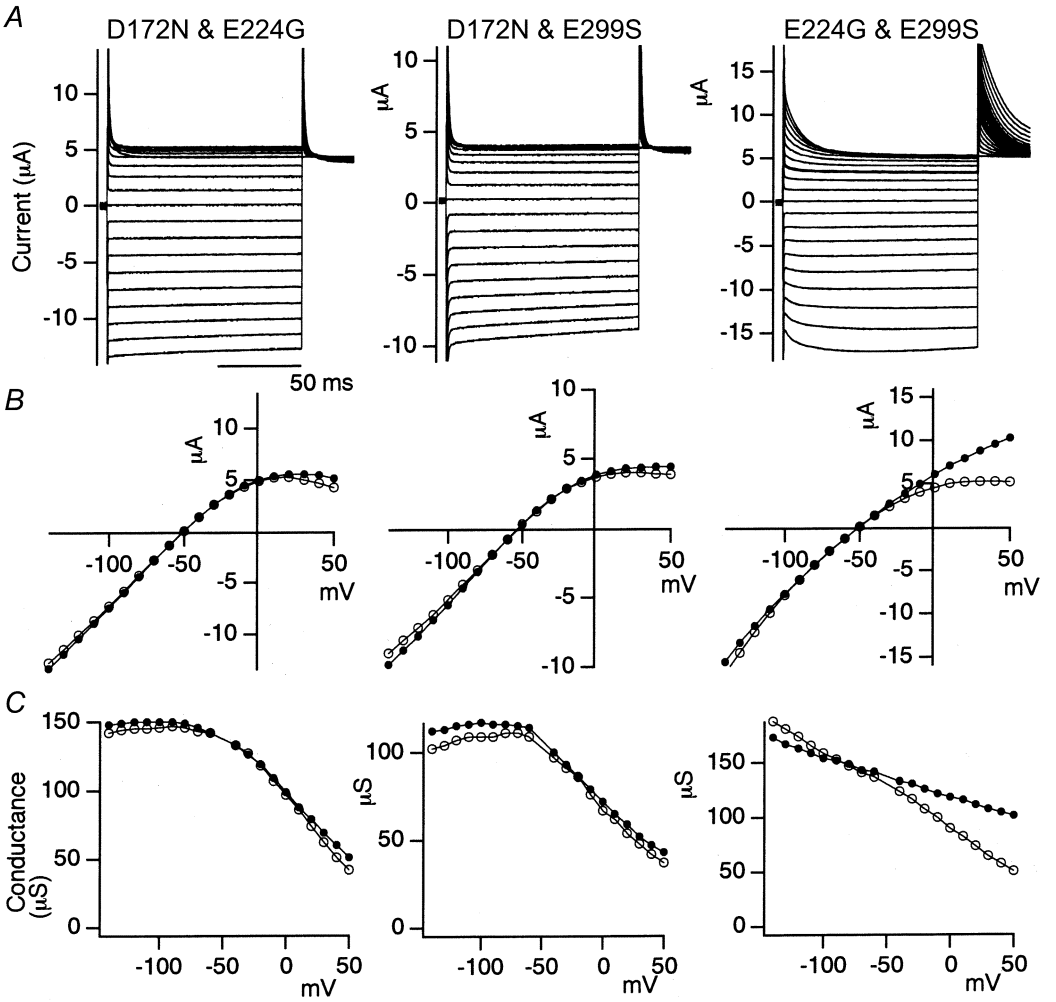

Figure 3. Macroscopic current recordings under two-electrode voltage clamp of double mutants of Kir2.1 (D172N–E224G, D172N–E299S and E224G–E299S) expressed in *Xenopus* oocytes

A detailed explanation is given in Fig. 2.

function. A triple-exponential function did not improve the fit. The two time constants obtained are plotted in Fig. 6*B*. The two time constants of E224G and E299S were in the same range, and those of E224G–E299S were much larger. These features were confirmed in three oocytes from the same batch, and also in other batches. The slight voltage dependency of the time constants (Fig. 6*B*) might be, at least partly, due to the artifact of the current measurements. The error due to the series resistance between the oocyte surface and the bath potential electrode was negligible for the conclusions drawn here.

Fraction of the slowly decaying component of the outward current of E224G–E299S

The slowly declining component of E224G–E299S did not increase proportionally as the amplitude of the preceding hyperpolarizing pulse increased. The amplitudes of the two components calculated in the fit of Fig. 6*B* are plotted in Fig. 6*C*. It is clear that the fast component increased monotonically and proportionally as the preceding step pulses were more hyperpolarized. In contrast, the increase in the amplitude of the slow component was not monotonic; the increase started to be augmented at −100 mV. These results were reproducibly observed in three oocytes from the same batch, and also in other batches.

If there is only a single open state (and no inactivated or blocked state) at the preceding hyperpolarized potentials, the ratio of the amplitudes of the fast and slow components would be expected to be independent of the preceding voltage steps. Therefore, the results in Fig. 6 imply that there are multiple states at hyperpolarized potentials in E224G–E299S and that the ratio of the probabilities of these states changes depending on the

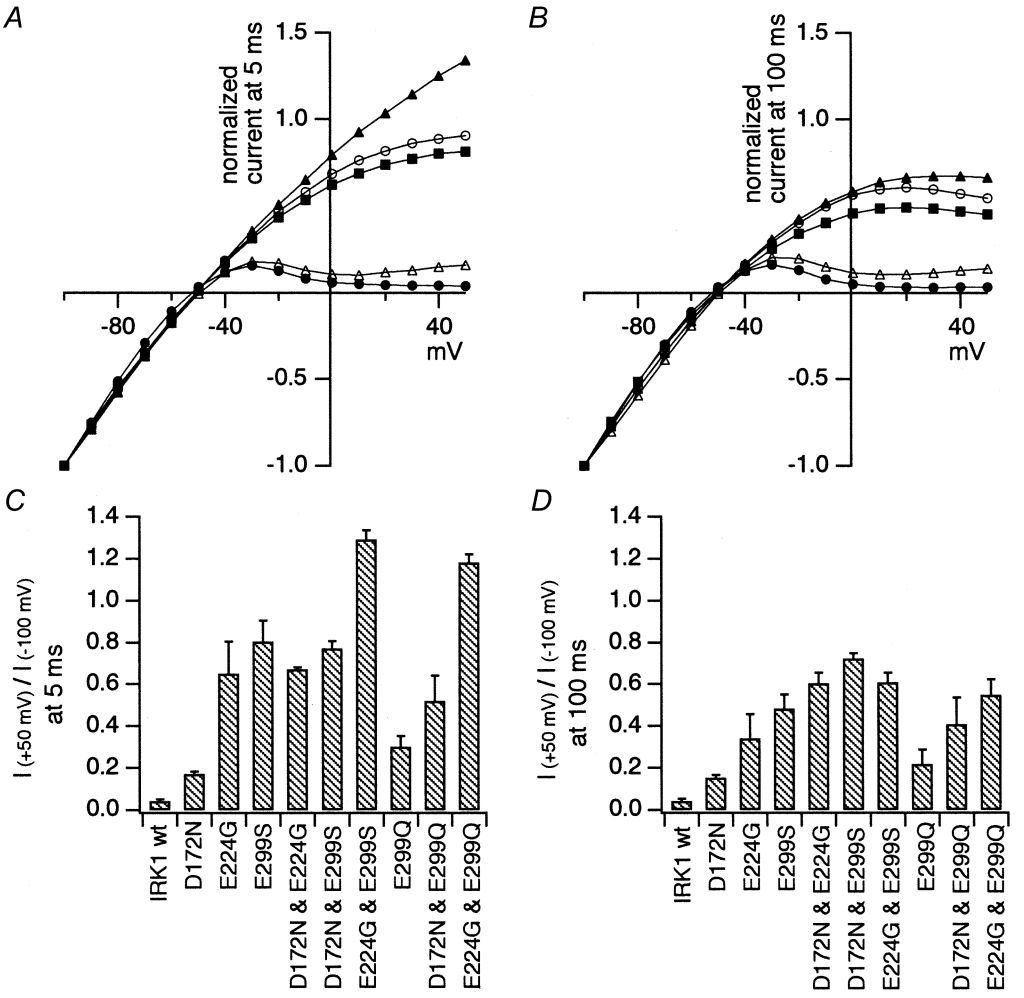

Figure 4. Comparison of the inward rectification properties of WT and mutant Kir2.1

A and *B*, the current amplitudes were normalized by those at −100 mV. The data at 5 ms (*A*) or 100 ms (*B*) from the beginning of the step pulses are plotted. The symbols used are as follows: WT, ●; D172N, △; E224G, ■; E299S, ○; E224G–E299S, ▲. *C* and *D*, the ratio of the current amplitudes at +50 and −100 mV was calculated as an index of the rectification intensity. The indexes at 5 ms (*C*) or at 100 ms (*D*) from the beginning of the step pulses are plotted. The mean and the standard deviation ($n = 3$–4) of each group are shown.

prepulse potential. A non-monotonic increase in the slow component was also noticed in E224G and in E299S (Fig. 6*A*).

Comparison of the sensitivity to the block by Mg_i^{2+} of WT and mutant Kir2.1

Kir2.1 WT and mutant cDNA was subcloned into the expression vector $pCXN_2$ and transfected to HEK293T cells by the lipofection method. The macroscopic current was recorded from excised inside-out membrane patches. The recordings, in the nominal absence of polyamines and in the presence of various concentrations of free Mg_i^{2+}, are shown in Fig. 7*A*. In the absence of polyamines and Mg_i^{2+}, the *I–V* relationships of WT and mutant Kir2.1 were almost linear over the time range studied. By increasing $[Mg^{2+}]_i$, the outward current of WT Kir2.1 at depolarized potentials was blocked almost instantaneously, but the outward current of the mutants was blocked much more slowly. The normalized *I–V* relationships at 500 ms from the beginning of the step pulses are plotted and the accumulated data of the inward rectification index in various $[Mg^{2+}]_i$ ($n = 3$–6) are shown in Fig. 7*B* and *C*, respectively. The normalized current amplitudes at 500 ms did not differ significantly between WT and the mutants.

The outward current amplitude and the inward rectification index of WT Kir2.1 in the absence of Mg_i^{2+} and polyamines showed high variation, as judged by the large standard deviation (Fig. 7*C*). As the sensitivity of the WT channels to block by spermine is extremely high as shown later, this variation is thought to be due to residual cytoplasmic polyamines, even after intensive perfusion of the bath (intracellular) solution with polyamine-free solution. The WT channel data in Fig. 7*A* and *B* in Mg_o^{2+}-free solution are from a case in which prominent outward current was observed.

Comparison of the sensitivity to block by spermine of WT and mutant Kir2.1

The current recordings in Fig. 8*A* were obtained in the absence of Mg_i^{2+} and in the presence of various concentrations of spermine, and the normalized *I–V* plots at 3 s from the beginning of the step pulses are shown in Fig. 8*B*. WT Kir2.1 was highly sensitive to block. E224G and E299S were much more resistant to block by spermine, and the decrease in sensitivity was even more prominent in E224G–E299S. These observations were confirmed in the accumulated data of the rectification index in Fig. 8*C* and *D* ($n = 3$–6). The sensitivities of E224G and E299S were approximately 100–1000 times lower

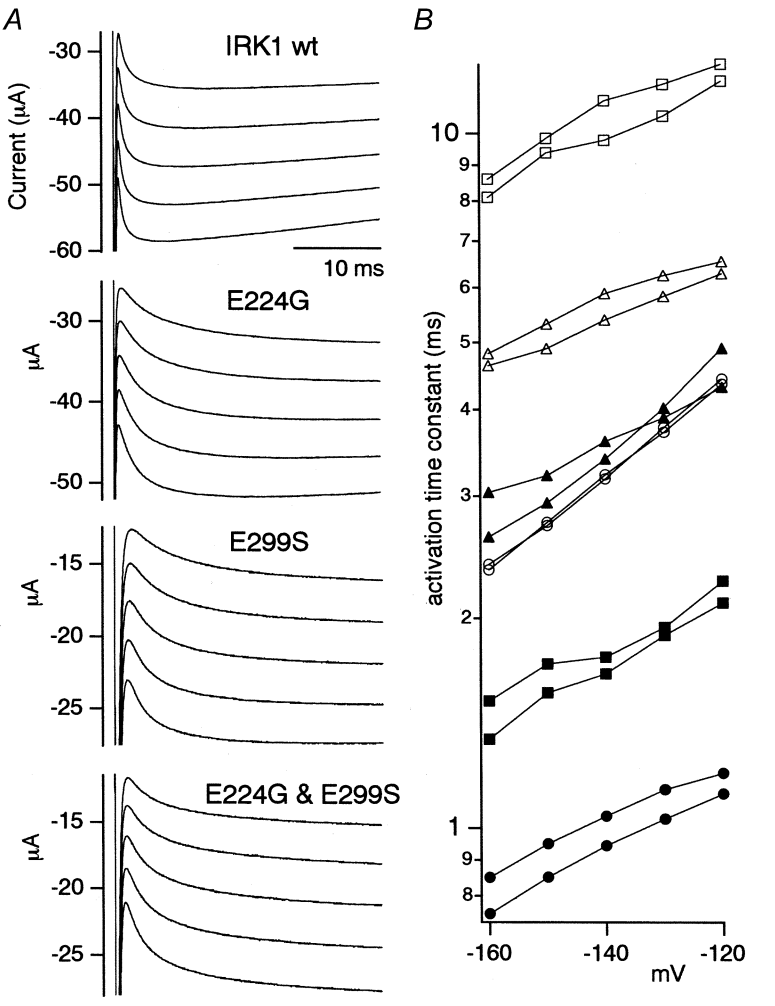

Figure 5. Comparison of the activation kinetics upon hyperpolarization of WT Kir2.1 and the E224G, E299S and E224G–E299S mutants expressed in *Xenopus* oocytes

A, current recordings at −120, −130, −140, −150 and −160 mV, hyperpolarized from 0 mV. $[K^+]_o$ was 10 mM. *B*, the activation phases were fitted with a single-exponential function and the time constants of the fits are plotted. The symbols used are as follows: WT Kir2.1, ●; E224G, ○; E299S, ▲; E224G–E299S, △. As there was a significant fitting error in the case of E224G–E299S, fitting with a double-exponential function was also done. The time constants for the fast (■) and the slow component (□) are also plotted. Data obtained from two oocytes from the same batch are shown for each channel.

than that of WT, and that of E224G–E299S was 10 000–100 000 times lower than that of WT (Fig. 8*C* and *D*). By fitting the data of Fig. 8*B*, the K_d values at +30 mV were estimated to be approximately 0.0005 μM for WT, 0.2 μM for E224G, 0.1 μM for E299S and 30 μM for E224G–E299S. The K_d value for the double mutant E224G–E299S assuming a simple additivity of changes in binding energy of E224G and E299S is predicted by the following equation: $K_{d(E224G-E299S)} = (K_{d(E224G)}K_{d(E299S)})/K_{d(WT)}$ (Yang *et al.* 1995). As the predicted value (40 μM) is close to the experimental value (30 μM), it is suggested that E224 and E299 contribute independently to spermine binding.

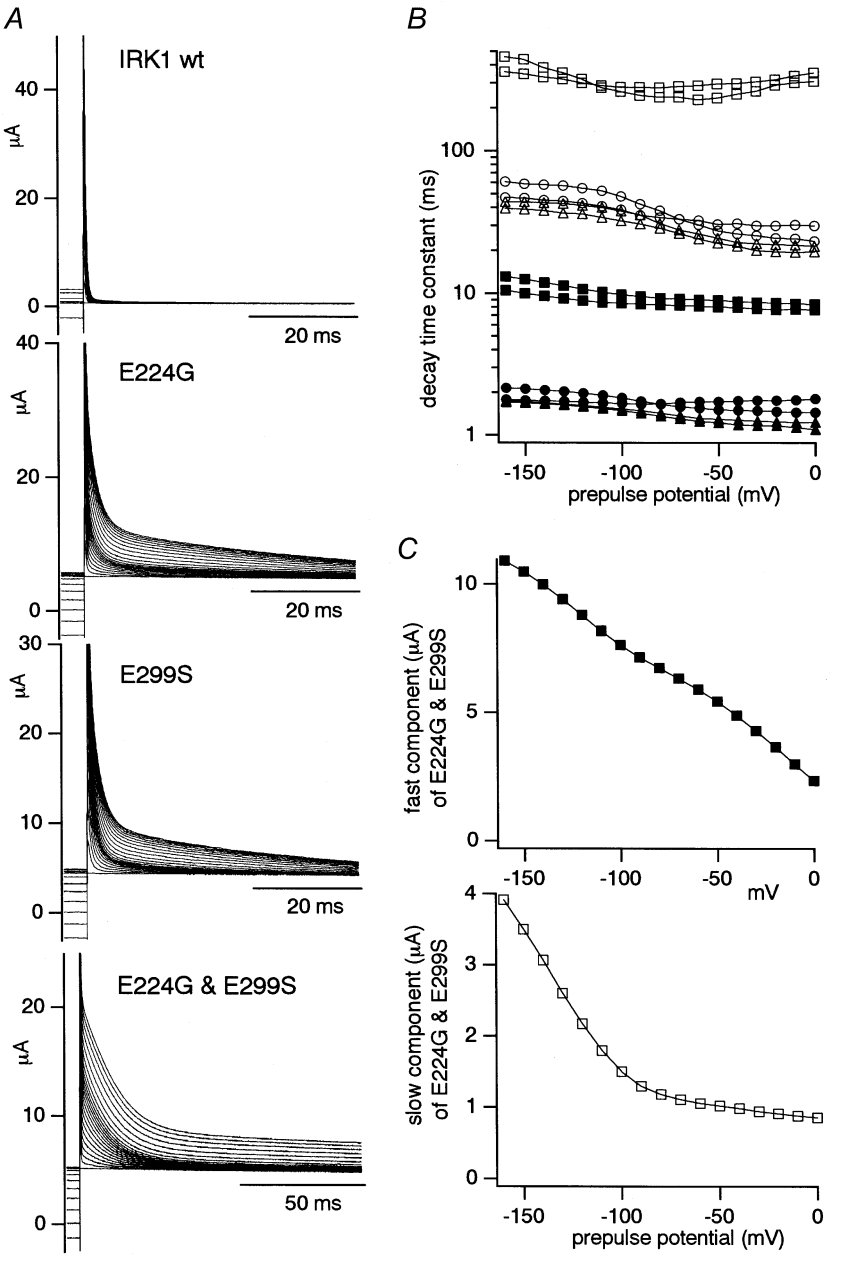

Figure 6. Comparison of the outward current of WT Kir2.1 and the E224G, E299S and E224G–E299S mutants expressed in *Xenopus* oocytes under two-electrode voltage clamp (*A* and *B*) and the dependency of the fraction of the slowly decaying component of E224G–E299S on the preceding step pulses

A, outward current recordings at +50 mV when depolarized from various potentials ranging from +50 to −160 mV. $[K^+]_o$ was 10 mM. *B*, the recordings of E224G, E299S and E224G–E299S were fitted with a double-exponential function, and the two time constants are plotted. The bottom axis indicates the voltage of the preceding step pulses. The symbols used are as follows: E224G, ●, ○; E299S, ▲, △; E299S–E224G, ■, □. The filled symbols represent the values of the fast component and the open symbols are for the slow one. Data from two oocytes from the same batch are plotted for each channel. *C*, the amplitudes of the fast (top) and the slow (bottom) components used for the fitting of E224G–E299S in *B*.

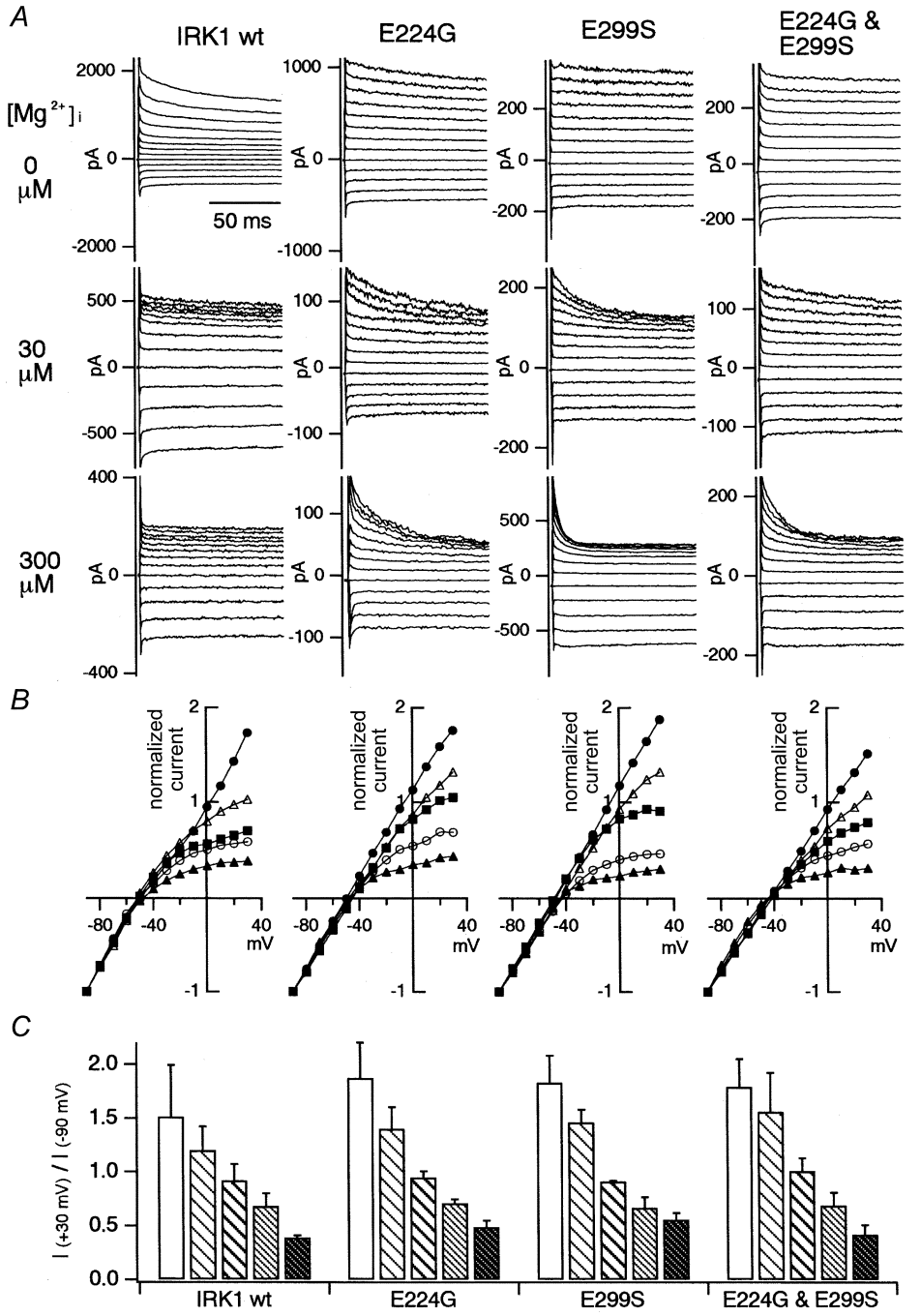

Figure 7. The sensitivity of the macroscopic currents of WT Kir2.1 and the E224G, E299S and E224G–E299S mutants to block by Mg_i^{2+}

A, macroscopic current recordings from an excised patch of HEK293T cells transfected with Kir2.1 WT or mutant cDNA. The concentration of free Mg_i^{2+} was determined by adding $MgCl_2$ and EDTA following the equation of Fabiato & Fabiato (1979). $[K^+]_o$ in the pipette was 20 mM, and $[K^+]_i$ in the bath was 140 mM. The calculated E_K was −49 mV. The holding potential was −50 mV and step pulses from +30 down to −90 mV were applied by 10 mV decrements. *B*, normalized *I–V* relationships at 500 ms from the beginning of the step pulses. The current amplitudes were normalized by the values at −90 mV. The symbols used are as follows: 0 μM Mg_i^{2+}, ●; 3 μM, △; 30 μM, ■; 300 μM, ○; 3 mM, ▲. *C*, comparison of the rectification indexes at 500 ms from the beginning of the step pulses. Rectification index was calculated as the ratio of the current amplitudes at +30 and −90 mV. The mean and the standard deviation of the accumulated data ($n = 3$–6) are plotted. The five bars indicate the values in 0, 3, 30, 300 and 3000 μM Mg_i^{2+}, from left to right.

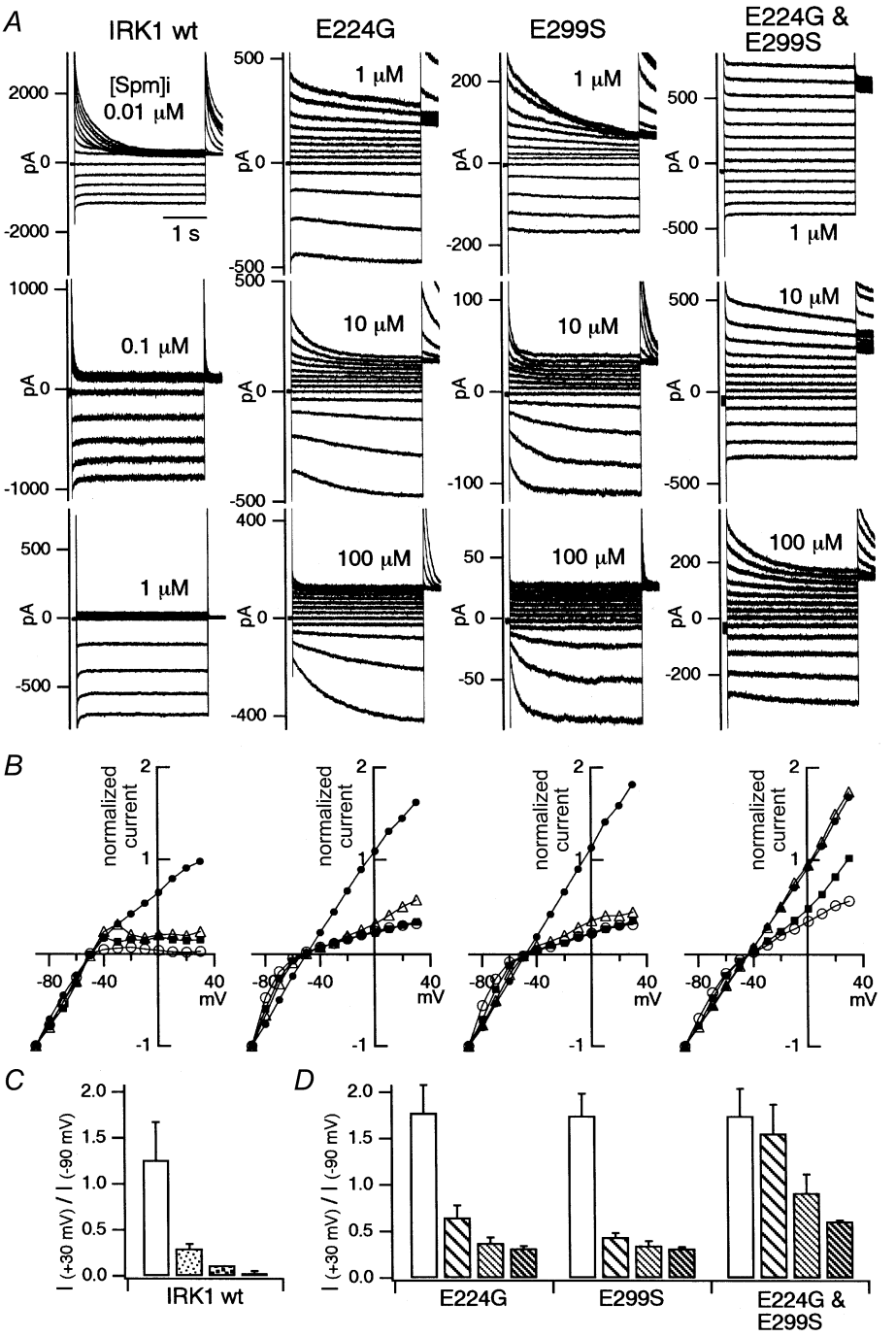

Figure 8. The sensitivity of the macroscopic current of WT Kir2.1 and the E224G, E299S and E224G–E299S mutants to block by spermine

A, macroscopic current recordings from an excised patch of HEK293T cells transfected with the channel cDNA. The concentrations of spermine (Spm) are indicated in each panel. Note that data for 0.01, 0.1 and 1 μM spermine are shown for WT Kir2.1, and data for 1, 10 and 100 μM spermine are shown for the mutants. $[K^+]_o$ and $[K^+]_i$ were 20 and 140 mM, respectively. The holding potential was −50 mV, and step pulses from +30 down to −90 mV were applied by 10 mV decrements. *B*, normalized *I–V* relationships at 3 s from the beginning of the step pulses. The current amplitudes were normalized to the values at −90 mV. The symbols used for WT are as follows: 0 μM, ●; 0.01 μM, △; 0.1 μM, ■; 1 μM, ○. The symbols for the mutants are as follows: 0 μM, ●; 1 μM, △; 10 μM, ■; 100 μM, ○. *C* and *D*, comparison of the rectification indexes at 3 s from the beginning of the step pulses. Rectification index was calculated as the ratio of the current amplitudes at +30 and −90 mV. The mean and the standard deviation ($n = 3$–6) are plotted. The four bars indicate the data in 0, 0.01, 0.1 and 1 μM spermine for WT (*C*), and 0, 1, 10 and 100 μM spermine for the mutants (*D*) from left to right.

Comparison of the single-channel conductance of WT and mutant Kir2.1

The single-channel recordings in Fig. 9*A* were obtained from *Xenopus* oocytes under the cell-attached patch configuration in 140 mM K_o^+ at −120 mV. The single-channel current–voltage relationships and the accumulated data for the single-channel conductance are shown in Fig. 9*B* and *C*. The values were (means ± S.D.) 19.7 ± 0.49 pS for WT, 16.7 ± 0.46 pS for E224G, 16.5 ± 0.35 pS for E299S and 12.7 ± 0.45 pS for E224G–E299S ($n = 3$). The open probability, the mean open time and the mean closed time did not show any obvious differences. Yang *et al.* (1995) reported that open channel noise is increased in the E224G mutant. A slight increase was also observed in the mutants of this study as shown in the expanded traces of Fig. 9*A* (right). The variance of the current fluctuation of the open channel at −120 mV was 0.024 pA^2 for WT, 0.050 pA^2 for E224G, 0.054 pA^2 for E299S and 0.032 pA^2 for E224G–E299S, when that of closed level was in the same range as follows: 0.014 pA^2 (WT), 0.012 pA^2 (E224G), 0.011 pA^2 (E299S) and 0.014 pA^2 (E224G–E299S). Taken together, these results suggest that E299 as well as E224 contribute to the permeation properties.

Phenotype of the D172N–E224G–E299S mutant and comparison with that of sWIRK

To examine whether the three sites focused on in the present study determine the inward rectification property completely, two triple mutants of Kir2.1, D172N–E224G–E299S and D172N–E224G–E299Q, were made. The E179Q mutant of sWIRK, which has no negative charges at the three sites in question (E179Q–G231–S311) were also made. The mutants were expressed in *Xenopus* oocytes and recorded in 10 mM K_o^+ under two-electrode voltage clamp. The current recordings

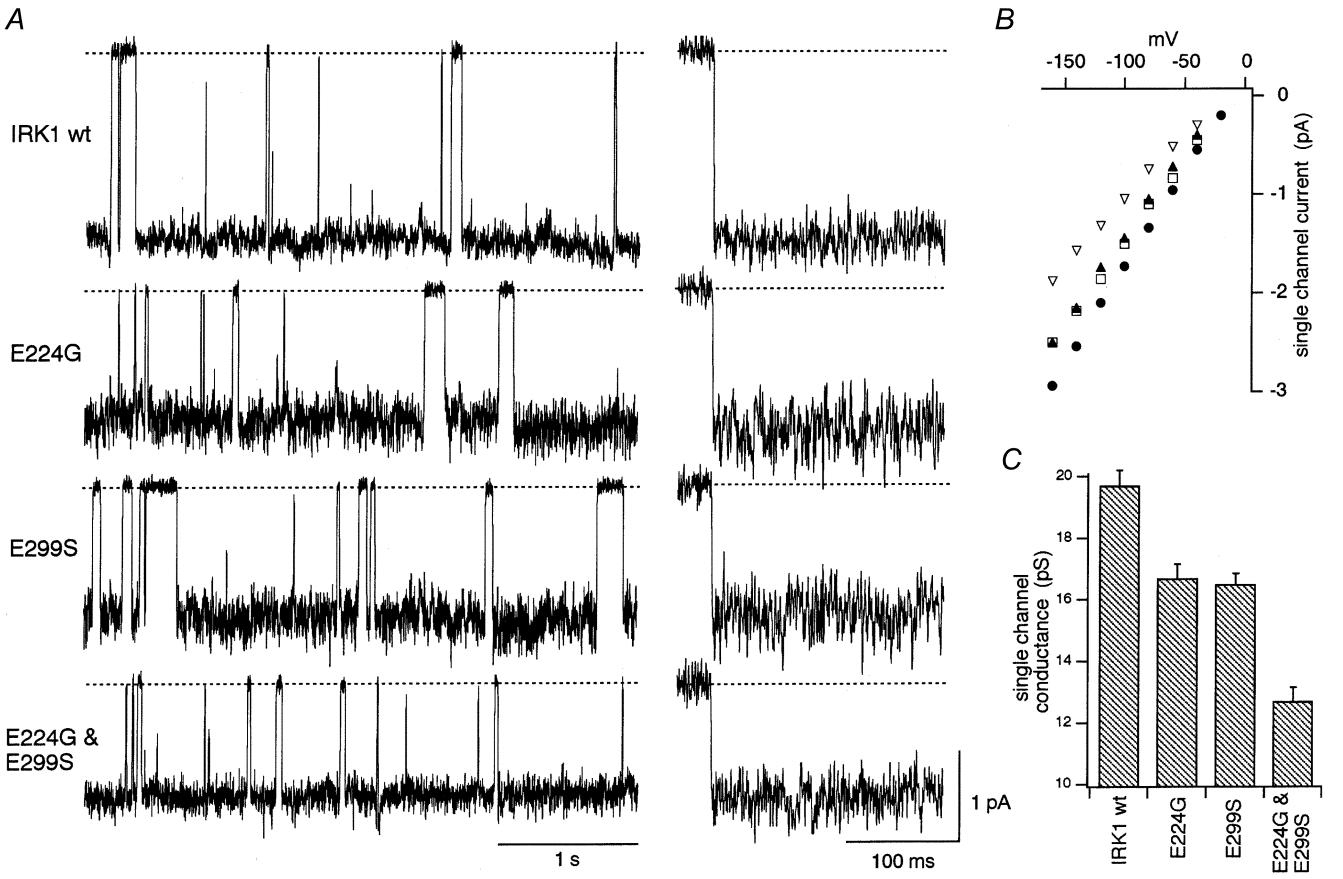

Figure 9. Comparison of the single-channel recordings of WT Kir2.1 and the E224G, E299S and E224G–E299S mutants

A, representative single-channel recordings in *Xenopus* oocytes under the cell-attached patch configuration. The $[K^+]_o$ in the pipette and in the bath was 140 mM. The holding potential of the displayed recordings was −120 mV. The dashed lines indicate the zero current level after subtracting the leak current. The traces are shown on an expanded time scale on the right to demonstrate the fluctuation of the open channel current. *B*, plot of the relationship of the single-channel current amplitude and the holding potential. The symbols used are as follows: WT Kir2.1, ●; E224G, ▲; E299S, □; E224G–E299S, ▽. *C*, the single-channel conductance calculated from the slope of the plot in *B*. The mean and the standard deviation ($n = 3$) are plotted.

(Fig. 10*A*), the *I–V* plots (Fig. 10*B*) and the *g–V* plots (Fig. 10*C*) are shown. As we reported previously (Kubo *et al.* 1996), E299Q of sWIRK showed a slight outward rectification, and no clear sign of inward rectification. The conductance at hyperpolarized potentials decreased. A kind of gating mechanism that leads to channel closure at negative voltages might explain this property. In contrast, a weak but clear inward rectification remained in the triple mutants of Kir2.1 (D172N–E224G–E299S and D172N–E224G–E299Q). The accumulated data ($n = 3$) of the rectification index support these observations (Fig. 10*D* and *E*).

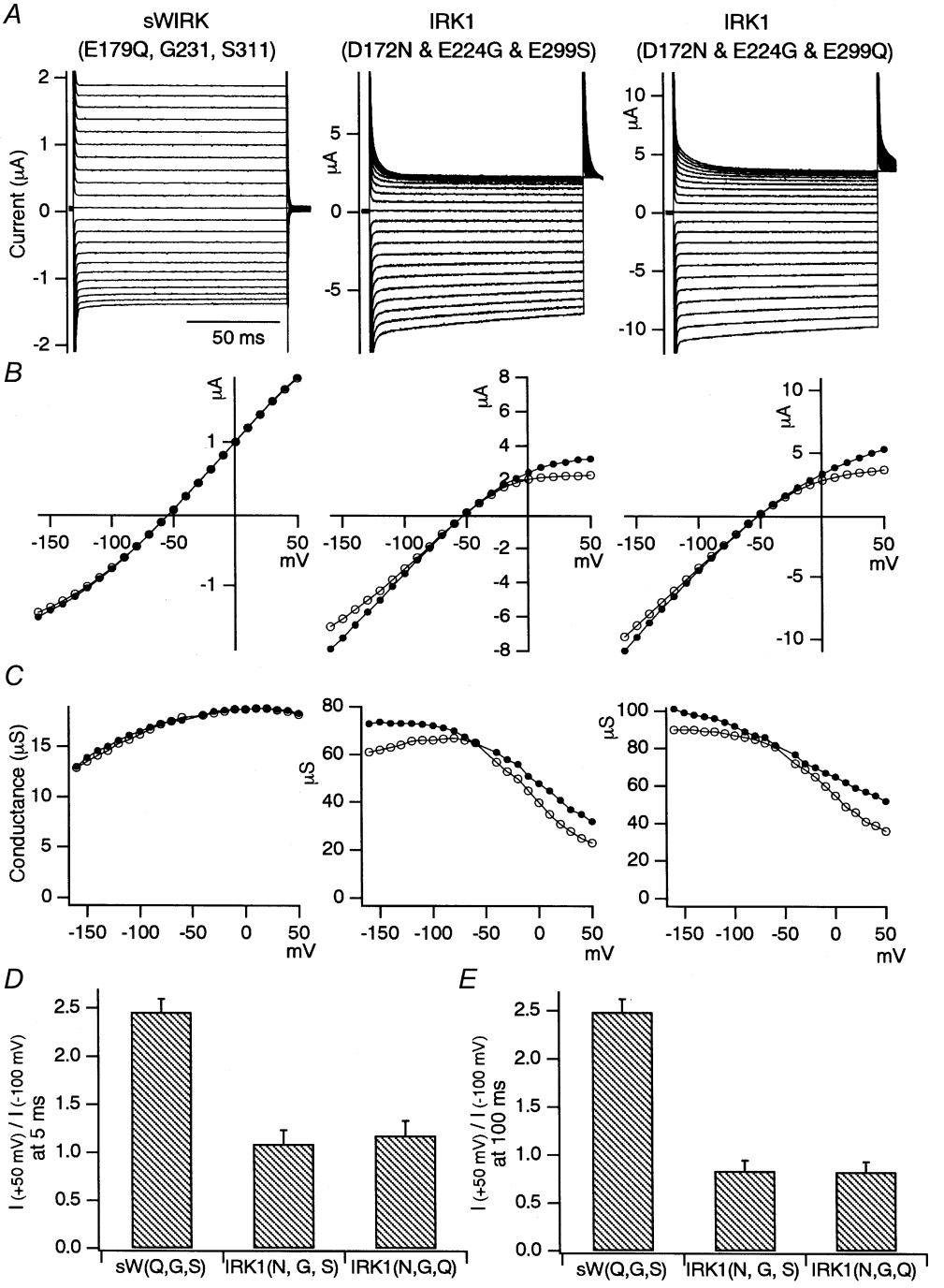

Figure 10. Macroscopic current recordings under two-electrode voltage clamp of the sWIRK mutant E179Q and two triple mutants of Kir2.1, D172N–E224G–E299S and D172N–E224G–E299Q, expressed in *Xenopus* oocytes

A detailed explanation of *A–C* is given in Fig. 2. *D* and *E*, the ratio of the current amplitudes at +50 and at −100 mV was calculated as an index of the rectification intensity. The mean and the standard deviation ($n = 3$) of the indexes at 5 ms (*D*) and at 100 ms (*E*) from the beginning of the step pulses are shown.

DISCUSSION

The difference between the intensity of inward rectification of Kir2.1 and that of sWIRK (Kubo *et al.* 1996) could not be explained by differences at the two sites already reported, D172 and E224. Therefore, the presence of an additional site(s) was postulated that contributes to the extent of the inward rectification. E299 of Kir2.1 in the region after M2 was newly identified in this study. The phenotypes of E224G and E299S were highly similar each other, and differed from that of WT Kir2.1 in terms of the rectification and permeation properties as follows. (1) The inward rectification was less intense (Figs 2–4). (2) The activation upon hyperpolarization was slower (Fig. 5). (3) The decay of the outward current at depolarized potentials was slower (Fig. 6). (4) The sensitivity to block of the outward current by spermine was severely reduced (Fig. 8). (5) The single-channel conductance was smaller (Fig. 9). Qualitatively similar but more enhanced changes were observed in the double mutant E224G–E299S.

The structure of the inner vestibule of Kir2.1

The observations above are surprising because E299 is located almost half-way through the long cytoplasmic chain after M2, and is very distant from E224 on the linear sequence (Fig. 1). In mutagenesis studies including Cys-scanning mutagenesis, there is always an argument that the mutagenesis effect might be due to drastic changes of the overall structure. Although this possibility remains in the present study, the relatively intact channel function of E299S and E299Q suggests that it is more straightforward to assume that the negative charges of E299 and E224 contribute to the permeation pathway. As no clear change of phenotype from WT could be observed in the E244Q mutant, the specificity of the effects of mutations at E299 and E224 was supported. Taking together the present results and the previous reports on E224 (Yang *et al.* 1995; Taglialatela *et al.* 1995; Nichols & Lopatin, 1997), it is likely that the cytoplasmic chain after M2 is infolded to comprise the inner vestibule, which is continuous with the membrane-spanning pore region, and that both E224 and E299 contribute to the permeation pathway (Fig. 11).

This speculation was supported by two recent reports by Lu *et al.* (1999*a*,*b*). They demonstrated by a stoichiometric covalent modification study that the inner vestibule of Kir2.1 is formed by both cytoplasmic amino- and carboxyl-terminal domains, and that the vestibule is spacious enough to fit multiple methanthiosulfonate reagents. They estimated the diameter to be larger than 12 Å even at the depth of D172. This image is quite different from the resolved pore structure of the bacterial two-transmembrane-type K^+ channel KcsA (Doyle *et al.* 1998). A difference between Kir2.1 and KcsA was also reported in the arrangement of the transmembrane segments (Minor *et al.* 1999) and in the pore structure (Thompson *et al.* 2000). Thompson *et al.* (2000) showed by mutagenesis study that residues beyond the selective filter of Kir2.1 channels contribute to permeation and blockage by extracellular cations, contrary to the expectations from the crystal structure of KcsA channels.

On the other hand, structural similarity between another inward rectifier channel Kir6.2 and KcsA was reported. Loussouarn *et al.* (2000) showed by Cys-scanning mutagenesis that at least three subunits are required to fit Cd^{2+}. Thus, they proposed that the inner vestibule of the pore of the Kir6.2 channel is relatively narrow, similar to that of the KcsA channel, and that it has a state-dependent flexibility. A high structural similarity of the KcsA to the Kir6.2 channel was also reported by modelling based on the KcsA structure (Capener *et al.* 2000). Taken together, there is still some controversy on the structure of Kir channels. This discrepancy might be partly due to the differences between Kir2.1 and Kir6.2. To have a conclusive understanding, we await the resolution of the structure of the Kir channel including the amino- and carboxyl-terminal regions in the crystal, because there is a possibility that the inner vestibule could be formed in a different way in the absence of these regions.

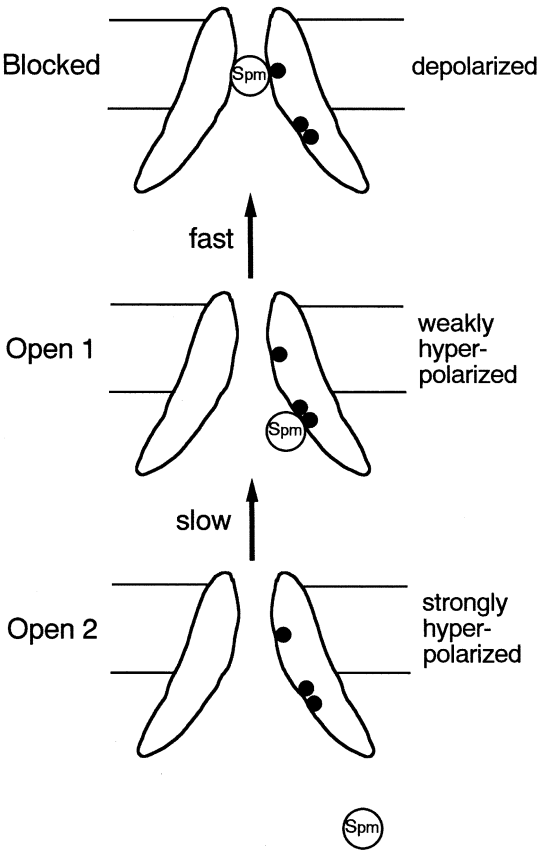

Figure 11. Scheme to explain the location and the functional role of E224G and E299S, and the possible presence of two open states

The upper filled circle depicts the position of D172, and two lower ones depict E224 and E299.

Differences between the functional role of D172 and those of E224 and E299

In the D172N mutant, the sensitivity to block by spermine was decreased and the activation phase at hyperpolarized potentials disappeared (Stanfield *et al.* 1994; Wible *et al.* 1994), suggesting that D172 has a strong energetic contribution to the binding of spermine in the channel pore. D172 was also reported to contribute to the binding of Mg^{2+} in the pore (Oishi *et al.* 1998). Thus, it is thought that D172 is a binding site or locates close to a binding site for these cytoplasmic blockers.

In the case of E224G, E299S and E224G–E299S, the sensitivity to block by spermine at depolarized potentials was much lower than that of WT (Fig. 8). In contrast with D172N, the activation speed at hyperpolarized potentials (unblocking) and the decay speed of the outward current at depolarized potentials (blocking) were slower than those of WT (Figs 5 and 6). Thus, we suggest that both the blocking and unblocking rates are decreased in these mutants, and that overall the effect of the mutation on the blocking rate is greater. If these residues were the pore-plugging binding site for spermine, the off-blocking rate in the mutants might be increased (i.e. the activation at hyperpolarized potentials might be faster). Therefore, E224 and E299 are unlikely to be the pore-plugging binding site for spermine. What then is the functional role of these sites?

One possibility is as follows. E224 and E299 are located at the inner vestibule and serve as an intermediate binding (and non-plugging) site which facilitates entry and exit of spermine to and from the final pore-plugging binding site located deeper in the pore. In the WT channel, the binding of spermine at the E224 and E299 level upon depolarization could result in an increase in the local concentration of spermine at the inner vestibule, and thus an increase in the on-blocking rate. Upon hyperpolarization, the presence of the intermediate binding (and non-plugging) site at the E224 and E299 level could facilitate the popping out of spermine from the D172 level, increasing the off-rate. Overall the effect on the blocking rate is much greater than the effect on the unblocking rate and so the blocking potency of spermine at depolarized potentials is dramatically enhanced with E224 and E299 in the WT. By mutating E224 and/or E299, the facilitating mechanisms described above for the entry and exit of spermine to and from the pore-plugging binding site may be affected, resulting in a dramatic decrease in both the blocking and the unblocking rates.

Two open states in the E224G–E299S double mutant

If the discussion on E224 and E299 in the previous section is true, there is a possibility that there exist two open states, namely one open state with no spermine in the inner vestibule and another conducting state with spermine at the E224 and/or E299 level. In the present study, data that are not contradictory with this possibility were obtained for the E224G–E299S mutant. As shown in Fig. 6, the fraction of the slowly decaying component of the outward current depended on the preceding prepulses. One possible interpretation, in which two open states were assumed, is shown schematically in Fig. 11. At less hyperpolarized potentials, spermine is released from the D172 level and the channel enters the open state. However, the released spermine still exists at the E224 and E299 levels. When depolarized back from the less hyperpolarized potential, the block of the outward current would proceed relatively fast, due to the high local concentration of spermine. In contrast, when strong hyperpolarization is applied, the cytoplasmic blocker would be released from the E224 and E299 level, and the local concentration of the blocker would be decreased. In this case, the blocking when depolarized would proceed only slowly. The same analysis could not be performed in WT Kir2.1, due to the very fast decay of the outward current. However, it is possible that a similar phenomenon to E224G–E299S occurs in WT Kir2.1.

In agreement with this discussion, Lee *et al.* (1999) also demonstrated the possibility that E224 functions as an intermediate binding (and non-plugging) point for spermine, by the combined use of spermine and a large spermine-related toxin which may reach the E224 level but not the D172 level. They argued that spermine binds first to the intrinsic gate close to E224, and then plugs the channel pore. Although Lee *et al.* (1999) assumed the intrinsic gate around E224 to be located in the cytoplasm, it is more likely that the carboxyl-terminal region including E224 (Yang *et al.* 1995) and E299 is folded to form the permeation pathway, because mutations at E224 and E299 affected the permeation properties (Fig. 9).

To explain the complex blocking behaviour of Kir2 channels by polyamines, a state model was proposed in which two binding sites for spermine were assumed (Lopatin *et al.* 1995; Guo & Lu, 2000). Lopatin *et al.* (1995) also produced a structural model in which two polyamines tandemly plug a long pore. It is possible that the deeper binding site is close to the D172 level and that the shallower one is close to the E224 and E299 levels. In the model by Lopatin *et al.* (1995), a state in which polyamine binds only to the shallower site was not postulated. It might correspond to the second open state discussed in the present study and by Lee *et al.* (1999).

Other amino acid residues for the control of inward rectification

There was a marked difference in the rectification property of E179Q of sWIRK (E179Q, G231, S311) and those of the triple mutants of Kir2.1 (D172N, E224G, E299S or Q) (Fig. 10), although both lack negatively charged amino acids at any of the three sites focused on in this study. It was also observed that the introduction of the S311E mutation to WT sWIRK (E179, G231, S311E)

or to the sWIRK E179Q mutant (E179Q, G231, S311E) did not significantly increase inward rectification (data not shown). The G231E mutation in WT sWIRK also did not clearly strengthen the inward rectification (data not shown). Taken together, these results suggest that the three sites are still insufficient to fully explain the intensity of the inward rectification, and that another important residue(s) for the strong inward rectification is missing in sWIRK. An amino acid residue just before M1 (M84 of Kir2.1), which was reported to be critical for the unblocking process (Ruppersberg *et al.* 1996), could not explain the difference between sWIRK and Kir1.1 because both of them have Lys at this residue. Further studies by systematic chimeras and mutants would provide a clue to a more conclusive understanding of this.

Bond, C. T., Pessia, M., Xia, X.-M., Lagrutta, A., Kavanaugh, M. P. & Adelman, J. P. (1994). Cloning and expression of a family of inward rectifier potassium channels. *Receptors and Channels* **2**, 183–191.

Capener, C. E., Shrivastava, I. H., Ranatunga, K. M., Forrest, L. R., Smith, G. R. & Sansom, M. S. P. (2000). Homology modeling and molecular dynamics simulation studies of an inward rectifier potassium channel. *Biophysical Journal* **78**, 2929–2942.

Dascal, N., Schreibmayer, W., Lim, N. F., Wang, W., Chavkin, C., Dimagno, L., Labarca, C., Kieffer, B. L., Gaveriaux-Ruff, C., Trollinger, D., Lester, H. & Davidson, N. (1993). Atrial G protein-activated K^+ channel: expression cloning and molecular properties. *Proceedings of the National Academy of Sciences of the USA* **90**, 10235–10239.

Doring, F., Derst, C., Wischmeyer, E., Karschin, C., Schneggenburger, R., Daut, J. & Karschin, A. (1998). The epithelial inward rectifier channel Kir7.1 displays unusual K^+ permeation properties. *Journal of Neuroscience* **18**, 8625–8636.

Doyle, D. A., Cabral, J. M., Pfuetzner, R. A., Kuo, A., Gulbis, J. M., Cohen, S. L., Chait, B. T. & MacKinnon, R. (1998). The structure of the potassium channel: Molecular basis of K^+ conduction and selectivity. *Science* **280**, 69–77.

Fabiato, A. & Fabiato, F. (1979). Calculator programs for computing the composition of the solutions containing multiple metals and ligands used for experiments in skinned muscle cells. *Journal de Physiologie* (*Paris*) **75**, 463–505.

Fakler, B., Brandle, U., Glowatzki, E., Weidemann, S., Zenner, H.-P. & Ruppersberg, J. P. (1995). Strong voltage-dependent inward rectification of inward rectifier K^+ channels is caused by intracellular spermine. *Cell* **80**, 149–154.

Ficker, E., Taglialatela, M., Wible, B. A., Henley, C. M. & Brown, A. M. (1994). Spermine and spermidine as gating molecules for inward rectifier K^+ channels. *Science* **266**, 1068–1072.

Guo, D. & Lu, Z. (2000). Mechanism of Kir2.1 channel block by intracellular polyamines. *Journal of General Physiology* **115**, 799–813.

Ho, K., Nichols, C. G., Lederer, W. J., Lyton, J., Vassilev, P. M., Kanazirska, M. V. & Hebert, S. C. (1993). Cloning and expression of an inwardly rectifying ATP-regulated potassium channel. *Nature* **362**, 31–38.

Iizuka, M., Kubo, Y., Tsunenari, I., Pan, C. X., Akiba, I. & Kono, T. (1995). Functional characterization and localization of a cardiac-type inwardly rectifying K^+ channel. *Receptors and Channels* **3**, 299–315.

Inagaki, N., Gonoi, T., Clement, J. P., Namba, N., Inazawa, J., Gonzalez, G., Aguilar-Bryan, L., Seino, S. & Bryan, J. (1995*a*). Reconstitution of I_{KATP}: an inward rectifier subunit plus the sulfonylurea receptor. *Science* **270**, 1166–1170.

Inagaki, N., Tsuura, Y., Namba, N., Masuda, K., Gonoi, T., Horie, M., Seino, Y., Mizuta, M. & Seino, S. (1995*b*). Cloning and functional characterization of a novel ATP-sensitive potassium channel ubiquitously expressed in rat tissues, including pancreatic islets, pituitary, skeletal muscle, and heart. *Journal of Biological Chemistry* **270**, 5691–5694.

Ishihara, K., Hiraoka, M. & Ochi, R. (1996). The tetravalent organic cation spermine causes the gating of the Kir2.1 channel expressed in murine fibroblast cells. *Journal of Physiology* **491**, 367–381.

Koyama, H., Morishige, K., Takahashi, N., Zanelli, J. S., Fass, D. N. & Kurachi, Y. (1994). Molecular cloning, functional expression and localization of a novel inward rectifier potassium channel in the rat brain. *FEBS Letters* **341**, 303–307.

Krapivinsky, G., Gordon, E. A., Wickman, K., Velimirovic, B., Krapivinsky, L. & Clapham, D. E. (1995). The G-protein-gated atrial K^+ channel I_{KACh} is a heteromultimer of two inwardly rectifying K^+ channel proteins. *Nature* **374**, 135–141.

Krapivinsky, G., Medina, I., Eng, L., Krapivinsky, L., Yang, Y. & Clapham, D. E. (1998). A novel inward rectifier K^+ channel with unique pore properties. *Neuron* **20**, 995–1005.

Kubo, Y. (1999). Structural bases for the inward rectification property of the Kir2.1 channel. *Japanese Journal of Physiology* **49**, suppl., S111.

Kubo, Y., Baldwin, T. J., Jan, Y. N. & Jan, L. Y. (1993*a*). Primary structure and functional expression of a mouse inward rectifier potassium channel. *Nature* **362**, 127–133.

Kubo, Y., Miyashita, T. & Kubokawa, K. (1996). A weakly inward rectifying potassium channel of the salmon brain: glutamate 179 in the second transmembrane domain is insufficient for strong rectification. *Journal of Biological Chemistry* **271**, 15729–15735.

Kubo, Y., Reuveny, E., Slesinger, P. A., Jan, Y. N. & Jan, L. Y. (1993*b*). Primary structure and functional expression of a rat G-protein-coupled muscarinic potassium channel. *Nature* **364**, 802–806.

Lee, J.-K., John, S. A. & Weiss, J. N. (1999). Novel gating mechanism of polyamine block in the strong inward rectifier K channel Kir2.1. *Journal of General Physiology* **113**, 555–563.

Lesage, F., Duprat, F., Fink, M., Guillemare, E., Coppola, T., Lazdunski, M. & Hugnot, J. P. (1994). Cloning provides evidence for a family of inward rectifier and G-protein coupled K^+ channels in the brain. *FEBS Letters* **353**, 37–42.

Lopatin, A. N., Makhina, E. N. & Nichols, C. G. (1994). Potassium channel block by cytoplasmic polyamines as the mechanism of intrinsic rectification. *Nature* **372**, 366–369.

Lopatin, A. N., Makhina, E. N. & Nichols, C. G. (1995). The mechanism of inward rectification of potassium channels: "Long-pore plugging" by cytoplasmic polyamines. *Journal of General Physiology* **106**, 923–955.

Loussouarn, G., Makhina, E. N., Rose, T. & Nichols, C. G. (2000). Structure and dynamics of the pore of inwardly rectifying K(ATP) channels. *Journal of Biological Chemistry* **275**, 1137–1144.

Lu, T., Nguyen, B. & Yang, J. (1999*a*). Cytoplasmic amino and carboxyl domains form a wide intracellular vestibule in an inwardly rectifying potassium channel. *Proceedings of the National Academy of Sciences of the USA* **96**, 9926–9931.

Lu, T., Nguyen, B., Zhang, X. & Yang, J. (1999*b*). Architecture of a K^+ channel inner pore revealed by stoichiometric covalent modification. *Neuron* **22**, 571–580.

Lu, Z. & MacKinnon, R. (1994). Electrostatic tuning of Mg^{2+} affinity in an inward-rectifier K^+ channel. *Nature* **371**, 243–246.

Matsuda, H. (1988). Open-state substructure of inwardly rectifying potassium channels revealed by magnesium block in guinea-pig heart cells. *Journal of Physiology* **397**, 237–258.

Matsuda, H., Saigusa, A. & Irisawa, H. (1987). Ohmic conductance through the inwardly rectifying K channel and blocking by internal Mg^{2+}. *Nature* **325**, 156–159.

Minor, D. L., Masseling, S. J., Jan, Y. N. & Jan, L. Y. (1999). Transmembrane structure of an inwardly rectifying potassium channel. *Cell* **96**, 879–891.

Nichols, C. G. & Lopatin, A. N. (1997). Inward rectifier potassium channels. *Annual Review of Physiology* **59**, 171–191.

Niwa, H., Yamamura, K. & Miyazaki, J. (1991). Efficient selection for high-expression transfectants with a novel eukaryotic vector. *Gene* **108**, 193–200.

Oishi, K., Omori, K., Ohyama, H., Shingu, K. & Matsuda, H. (1998). Neutralization of aspartate residues in the murine inwardly rectifying K^+ channel Kir2.1 affects the substate behaviour in Mg^{2+} block. *Journal of Physiology* **510**, 675–683.

Ruppersberg, J. P., Fakler, B., Brandle, U., Zenner, H. P. & Schultz, J. H. (1996). An N-terminal site controls blocker-release in Kir2.1 channels. *Biophysical Journal* **70**, A361.

Sabirov, R. Z., Tominaga, M., Miea, A., Okada, Y. & Oiki, S. (1997). A conserved arginine residue in the pore region of an inward rectifier K channel (IRK1) as an external barrier for cationic blockers. *Journal of General Physiology* **110**, 665–677.

Stanfield, P. R., Davies, N. W., Shelton, P. A., Sutcliffe, M. J., Khan, I. A., Brammer, W. J. & Conley, E. C. (1994). A single aspartate residue is involved in both intrinsic gating and blockage by Mg^{2+} of the inward rectifier, Kir2.1. *Journal of Physiology* **478**, 1–6.

Taglialatela, M., Ficker, E., Wible, B. A. & Brown, A. M. (1995). C-terminus determinants for Mg^{2+} and polyamine block of the inward rectifier K^+ channel Kir2.1. *EMBO Journal* **14**, 5532–5541.

Takumi, T., Ishii, T., Horio, Y., Morishige, K., Takahashi, N., Yamada, M., Yamashita, T., Kiyama, H., Sohmiya, K., Nakanishi, S. & Kurachi, Y. (1995). A novel ATP-dependent inward rectifier potassium channel expressed predominantly in glial cells. *Journal of Biological Chemistry* **270**, 16339–16346.

Thompson, G. A., Leyland, M. L., Ashmole, I., Sutcliffe, M. J. & Stanfield, P. R. (2000). Residues beyond the selectivity filter of the K^+ channel Kir2.1 regulate permeation and block by external Rb^+ and Cs^+. *Journal of Physiology* **526**, 231–240.

Topert, C., Doring, F., Wischmeyer, E., Karschin, C., Brockhaus, J., Ballanyi, K., Derst, C. & Karschin, A. (1998). Kir2.4: a novel K^+ inward rectifier channel associated with motoneurons of cranial nerve nuclei. *Journal of Neuroscience* **18**, 4096–4105.

Vandenberg, C. A. (1987). Inward rectification of a potassium channel in cardiac ventricular cells depends on internal magnesium ions. *Proceedings of the National Academy of Sciences of the USA* **84**, 2560–2564.

Watanabe, S.-I., Kusama-Eguchi, K., Kobayashi, H. & Igarashi, K. (1991). Estimation of polyamine binding to macromolecules and ATP in bovine lymphocytes and rat liver. *Journal of Biological Chemistry* **266**, 20803–20809.

Wible, B. A., Taglialatela, M., Ficker, E. & Brown, A. M. (1994). Gating of inwardly rectifying K^+ channels localized to a single negatively charged residue. *Nature* **371**, 246–249.

Yang, J., Jan, Y. N. & Jan, L. Y. (1995). Control of rectification and permeation by residues in two distinct domains in an inward rectifier K^+ channel. *Neuron* **14**, 1047–1054.

Acknowledgements

The authors would like to thank Dr J. Miyazaki (Osaka University) for the $pCXN_2$ expression vector, and Drs K. Ishihara (Saga Medical School), S. Oiki (Fukui Medical School) and K. Takahashi (Meiji University of Pharmacy) for invaluable suggestions and discussion. This work was supported in part by research grants from the Ministry of Education, Science, Sports and Culture, Japan and from the Mitsubishi Foundation.

Corresponding author

Y. Kubo: Department of Physiology, Tokyo Medical and Dental University, Graduate School and Faculty of Medicine, Yushima 1-5-45, Bunkyo-ku, Tokyo 113-8519, Japan.

Email: ykubo.phy2@med.tmd.ac.jp